RSC Advances

PAPER

View Article Online
View Journal | View Issue

Cite this: *RSC Adv.*, 2022, **12**, 26895

In vitro and computational investigations of novel synthetic carboxamide-linked pyridopyrrolopyrimidines with potent activity as SARS-CoV-2-M^{Pro} inhibitors†

Ateyatallah Aljuhani,‡[a] Hany E. A. Ahmed,‡*[bc] Saleh K. Ihmaid,[bd] Abdelsattar M. Omar,[efg] Sultan S. Althagfan,[h] Yaser M. Alahmadi,[h] Iqrar Ahmad,[i] Harun Patel,[i] Sahar Ahmed,[bj] Mohannad A. Almikhlafi,[k] Ahmed M. El-Agrody,[l] Mohamed F. Zayed,[gm] Safaa Abdulrahman Turkistani,[m] Shorouk H. Abulkhair,[p] Mohammed Almaghrabi,[b] Samir A. Salama,[n] Ahmed A. Al-Karmalawy[o] and Hamada S. Abulkhair *[co]

An essential target for COVID-19 is the main protease of SARS-CoV-2 (M^{pro}). With the objective of targeting this receptor, a novel set of pyrido[1,2-*a*]pyrrolo[2,3-*d*]pyrimidines with terminal carboxamide fragments was designed, synthesized, and considered as an initial motif for the creation of effective pan-coronavirus inhibitors. Accordingly, nine derivatives (**21–29**) have been introduced for *in vitro* assay to evaluate their antiviral activity and cytotoxicity effect against COVID-19 virus using Vero cells. The obtained data revealed that the majority of these derivatives showed potent cellular anti-COVID-19 activity and prevent viral growth by more than 90% at two different concentrations with weak or even no detectable cytotoxic effect on Vero cells. Extensive molecular docking simulations highlighted proper non-covalent interaction of new compounds within the binding pocket of M^{pro} as a potential target for their antiviral activity. *In vitro* assay for all the synthesized derivatives against the viral M^{pro} target indicated that compounds **25** and **29** have promising inhibitory activity with IC_{50} values at low micromolar concentrations. The molecular dynamic simulation results predicted the stability of compound **29** in the binding cavity of SARS-CoV-2 M^{pro} and hence supported the high inhibitory activity shown by the *In vitro* assay. These results suggested that compounds **25** and **29** merit further investigations as promising drug candidates for the management of SARS-CoV-2.

Received 29th June 2022
Accepted 12th September 2022

DOI: 10.1039/d2ra04015h

rsc.li/rsc-advances

[a]*Chemistry Department, College of Sciences, Taibah University, Al-Madinah Al-Munawarah 41477, Saudi Arabia*

[b]*Pharmacognosy and Pharmaceutical Chemistry Department, College of Pharmacy, Taibah University, Al-Madinah Al-Munawarah, Saudi Arabia*

[c]*Pharmaceutical Organic Chemistry Department, Faculty of Pharmacy, Al-Azhar University, Nasr City 11884, Cairo, Egypt. E-mail: hamadaorganic@azhar.edu.eg*

[d]*Pharmaceutical Chemistry Department, Faculty of Pharmacy, Jadara University, Irbid, Jordan*

[e]*Department of Pharmaceutical Chemistry, Faculty of Pharmacy, King Abdulaziz University, Alsulaymanyah, Jeddah 21589, Saudi Arabia*

[f]*Center for Artificial Intelligence in Precision Medicines, King Abdulaziz University, Jeddah 21589, Saudi Arabia*

[g]*Department of Pharmaceutical Chemistry, Faculty of Pharmacy, Al-Azhar University, Nasr City 11884, Cairo, Egypt*

[h]*Clinical and Hospital Pharmacy Department, College of Pharmacy, Taibah University, Al-Madinah Al-Munawarah, Saudi Arabia*

[i]*Division of Computer Aided Drug Design, Department of Pharmaceutical Chemistry, R. C. Patel Institute of Pharmaceutical Education and Research, Shirpur, 425405, Maharashtra, India*

[j]*Department of Medicinal Chemistry, Faculty of Pharmacy, Assiut University, Assuit, Egypt*

[k]*Pharmacology and Toxicology Department, College of Pharmacy, Taibah University, Al-Madinah Al-Munawarah, Saudi Arabia*

[l]*Chemistry Department, Faculty of Science, Al-Azhar University, Nasr City, Cairo, Egypt*

[m]*Pharmaceutical Sciences Department, Fakeeh College for Medical Sciences, Jeddah 21461, Saudi Arabia*

[n]*Division of Biochemistry, Department of Pharmacology, College of Pharmacy, Taif University, P.O. Box 11099, Taif 21944, Saudi Arabia*

[o]*Pharmaceutical Chemistry Department, Faculty of Pharmacy, Horus University – Egypt, International Coastal Road, New Damietta 34518, Egypt*

[p]*Department of Biochemistry, Faculty of Medicine, Al-Azhar University (Girls), Nasr City 11754, Cairo, Egypt*

† Electronic supplementary information (ESI) available. See https://doi.org/10.1039/d2ra04015h

‡ These authors contributed equally to this work and share first authorship.

Introduction

Coronavirus disease (COVID-19) is a life-threatening infectious disease caused by the Severe Acute Respiratory Syndrome Coronavirus 2 (SARS-CoV-2), which was discovered first in Wuhan city in China and subsequently spread worldwide.[1] Based on the epidemiological report of the WHO on 21 June 2022 there have been more than 537 500 000 confirmed cases of COVID-19, including 6 319 395 confirmed deaths globally.[2] Until the end of 2021, there was no approved specific antiviral drug for treatment, and all options were based on symptomatic treatment and oxygen therapy to manage respiratory impairment. Recently, the Food and Drug Administration (FDA) has authorized the combination of nirmatrelvir and ritonavir for the emergency use only in mild-to-moderate cases of COVID-19. Consequently, there is still unmet needs for effective treatment options against the SARS-CoV-2 virus. One strategy that has been followed by scientists to combat the widespread of new viral strains is to use the already approved antiviral medications.[3–5] Most of the currently used antiviral drugs are nucleoside analogs[6] such as Remdesivir (**1**; Fig. 1), Ribavirin (**2**), Sofosbuvir (**3**), Galidesivir (**4**), and Tenofovir (**5**).

Despite the recommendation of such antiviral agents together with the antibacterial and other antiviral medications azithromycin, molnupiravir (**6**), and favipiravir (**7**) to manage the emergency cases, no effective drug has yet been introduced to treat specific structures of viral components of SARS-CoV-2.[7] The main protease M^{pro} (also called $3CL^{pro}$) of coronavirus is a key mediator in viral replication and transcription. This functional importance, together with the absence of a closely related analogous target in humans, made the SARS-CoV-2 main protease M^{pro} an interesting target for the design of antiviral agents.[5,8,9] Consequently, many attempts have been adopted to develop M^{pro} inhibitor-based antiviral medication. As a result, a number of antiviral agents with prominent activity against SARS-CoV-2 were discovered. These include boceprevir (**8**) and GC-376 (**9**) which were verified as inhibitors of M^{pro} through binding to its catalytic active site.[10]

Computational methods play an important role in the design of novel M^{pro} antagonistic drugs.[4,11–14] In this context, a structure-based virtual screening was conducted by Jin and co-workers to evaluate a library of more than 10 000 well-known compounds as potential inhibitors of M^{pro}.[15] Among compounds of the tested library, six inhibited M^{pro} with IC_{50} values range of 0.67–21.4 μM.[16] Additionally, MUT056399 (**10**; Fig. 2) has been identified as a carboxamide-incorporating inhibitor of SARS-CoV-2-M^{Pro} with an EC_{50} value of 38.24 μM with the preferential quality of low cytotoxicity (CC_{50} > 100 μM). The carboxamide group of this latter forms two hydrogen bonds with the amino acid residues His163 and Phe140 in the S1 subsite of SARS-CoV-2-M^{Pro}.[17,18] ZINC02123811 (**11**) is another carboxamide derivative derived from a natural source and has the affinity to bind with the active pocket of SARS-CoV-2 M^{pro}.[19] The root-mean-square fluctuation (RMSF) analysis indicates that the complex of M^{pro} with this carboxamide derivative is pretty stable all over the simulation course.

On the other hand, pyridine, pyrimidine, and pyrrole have long been considered privileged fragments in the construction of antiviral candidates and potential inhibitors of SARS-CoV-2-M^{Pro} in particular.[20,21] Compound **12** is a pyridine derivative that has been evaluated for its activity against the Frankfurt-1 strain of SARS-CoV by MTT assay in Vero E6 cells. Results of the antiviral evaluation displayed a good potency and selectivity of **12** toward SARS-CoV-2-M^{Pro} with an IC_{50} value of 0.50 μM.[22] *In silico* docking studies were also performed on compound **13** against the binding pocket of SARS-CoV-2-M^{Pro}. Results suggested that it is a promising anti-SARS-CoV agent (IC_{50} = 30 nM), and revealed a good fitting within the active site of the protein target through the formation of three hydrogen bonds with the amino acid residues Cys145, Ser144, and Gly143.[23] Investigating the inhibitory potency of the pyrimidine-based molecule **14** against SARS-CoV-M^{Pro} demonstrated its good activity with an IC_{50} value of 6.10 μM.

Rationale and aim of the work

High-throughput screening of a library of small synthetic molecules against the infectious hepatitis C virus (HCV)

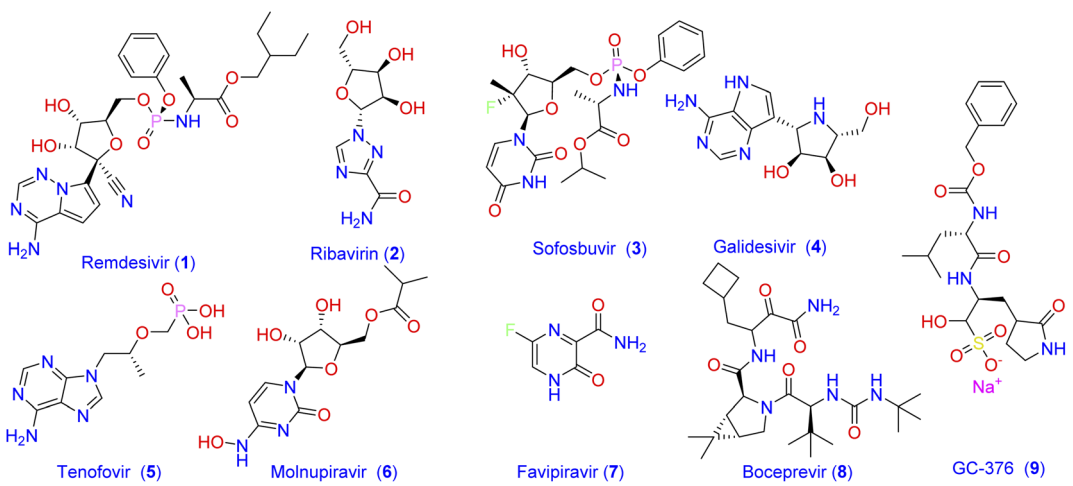

Fig. 1 Frequently prescribed antiviral drugs and recently identified molecules with prominent activity against SARS-CoV-2.

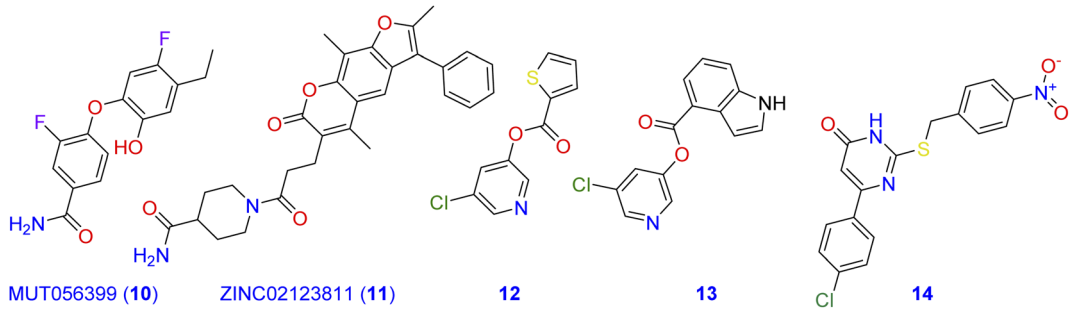

Fig. 2 Carboxamide, pyridine, and pyrimidine incorporating molecules with potent SARS-CoV-2-M^{Pro} antagonistic activity.

identified the iminodipyridinopyrimidine (IDPP; Fig. 3) scaffold as a potent inhibitor in the early and the late steps of the HCV lifecycle.[24,25] This scaffold showed also high levels of safety and metabolic stability. The 3D structure of HCV protease has a high level of similarity with the SARS-CoV-2-M^{Pro} (Z score = +8.40).[26,27] Like M^{pro}, the HCV protease also has a double β-barrel fold, with relatively similar orientations to those of the SARS-CoV-2 M^{pro}, and a substrate-binding site located in a shallow cleft between its two six-to eight-stranded antiparallel β-barrels.[28] The superimposition of these two proteases suggested the superimposition of their substrate binding pockets and their active-site catalytic residues.[28,29] Accordingly, the IDPP scaffold is suggested to have a broad antiviral spectrum against both HCV and SARS-CoV-2-M^{Pro}. In continuation to our recent reports on the design of suggested bioactive molecules,[30–33] the objective of the current research is to modify the structure of the reported HCV antiviral agents IDPP into pyridopyrrolopyrimidine new scaffolds and to assess the potential of new candidates to inhibit SARS-CoV-2-M^{Pro}. Hence, while keeping the carboxamide functionality linked to the new scaffold, two structural modifications of IDPP analog were conducted to enhance the ligand binding and consequently the potency: the six-membered pyridine-imine fragment was replaced with the pyrrole aromatic system; the benzyl substituent attached to the pyridine-nitrogen was replaced with a smaller hydrophobic moiety. Accordingly, the new scaffold possesses the advantages of incorporating the privileged fragments pyridine, pyrimidine, pyrrole, and carboxamide which have been reported as pharmacophoric groups in certain SARS-CoV-2-M^{Pro} inhibitors.[20,21,34] A set of *in vitro* biological evaluation studies has been performed. The effect of new compounds to inhibit the viral replication of SARS-CoV-2 and antagonize its main protease was evaluated. As well, cell growth inhibition after treatment with new ligands has been assessed. A structure-

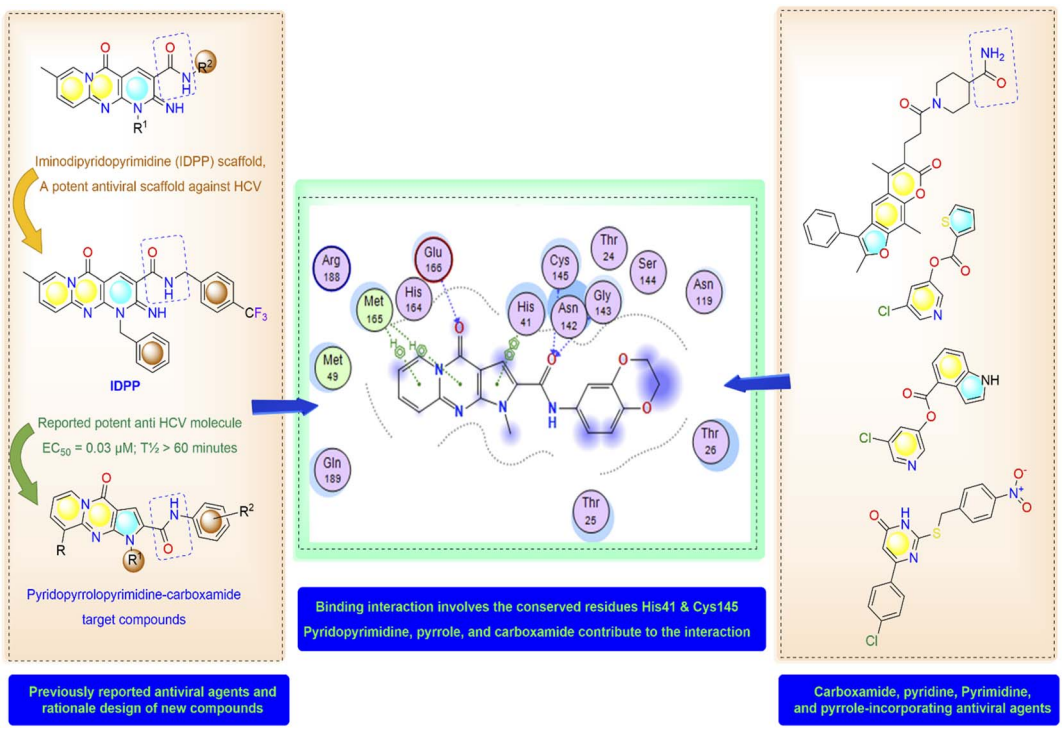

Fig. 3 Molecular design and rationale analysis for the binding interactions of novel pyridopyrrolopyrimidines within active pocket of SARS-CoV-2-M^{Pro}.

based approach was utilized using molecular docking simulation of the reported active IDPP analog compared to the newly designed pyridopyrrolopyrimidines within the M^{pro} protease target of SARS-CoV; PDB 7L11. The pre-docking screening of designed ligands within the protease binding pocket (Fig. 3) showed three promising findings: (1) an edge-to-face aryl–aryl interaction with the catalytic residue His41; (2) terminal amide carbonyl is directed well at the NH of Cys145; (3) the carbonyl of the fused system appears with proper placement with the polar environment, including the side chains of Met165, His164, and Glu166. In contrast, the behavior of IDPP analog with pyridine-imine part fails to participate in the good orientation of fused system through these major and conserved interactions within the pocket due to loss of aromaticity and false ordinations of terminal amide and the carbonyl group of fused system. Moreover, there is an unfavorable benzyl substitution attached to the pyridine-N that is located at the polar binding pocket. Molecular dynamic simulations were used for confirming these findings and measuring the stability within the pocket.

Results and discussion

Chemistry

In order to elucidate the scope and features of the cyclization reaction, the starting methyl-1-benzyl/methyl-4-oxo-1,4-dihydropyrido[1,2-*b*]pyrrolo[2,3-*d*]pyrimidine-2-carboxylate and its 9-methyl derivatives (**17, 18**) were prepared in moderate to good yields by the reaction of 2-chloro-4-oxo-4*H*-pyrido[1,2-*a*]pyrimidine-3-carbaldehyde[35] and its 9-methyl derivatives (**15, 16**) with amino acid methyl esters namely, methyl-*N*-methyl(*N*-benzyl)glycinate or methyl methyl-*N*-benzyl glycinate in a mixture of methanol and triethylamine under reflux as shown in Scheme 1. Hydrolysis of the ester derivatives **17, 18** by aqueous lithium hydroxide affords the corresponding intermediate, 1-benzyl/methyl-4-oxo-1,4-dihydro-pyrido[1,2-*a*]pyrrolo[2,3-*d*]pyrimidine-2-carboxylic acid and its 9-methyl derivatives (**19, 20**). Condensation of these carboxylic acid intermediates with appropriate aniline derivatives in the presence of 1,1′-carbonyldiimidazole (CDI) and acetonitrile gives the target *N*-aryl-1-benzyl/methyl-4-oxo-1,4-dihydropyrido[1,2-*a*]pyrrolo[2,3-*d*]pyrimidine-2-carboxamides (**21–29**) as shown in Scheme 1 with different substitutions on the original scaffold at N-1 and carboxamide functionality.

Spectroscopic data

The ^{1}H-NMR spectra of **21–29** showed singlet signals attributable to NH proton of the carboxamide functionality at the regions of 10.85–11.12 ppm. Moreover, compounds **21–29** exhibited the signals of the methylene and *N*-methyl group protons at δ 5.88 and δ 4.01–4.09, respectively. In addition, the elemental analysis and mass spectra of compounds **21–29** confirmed their proposed structures, see ESI†.

Biological screening

Evaluation of antiviral activity against SARS-CoV-2. The antiviral activity of compounds (**17**, and **21–29**) was screened in plated Vero E6 cells (CCL-8; ATCC origin provided by the Virology Sector, VACSERA, Giza, Egypt; https://www.vacsera.com/) and infected later with SARS-CoV-2 at a multiplicity of infection (MOI) of 0.01. The % inhibition of viral replication was measured applying two analogs' concentrations: 1 and 10 μM. In addition, the concentrations required to inhibit virus replication by 50% effective inhibitory concentration (EC_{50}) were calculated using five different concentrations by fitting a sigmoidal curve to the data following the logarithmic transformation of the drug concentration. In

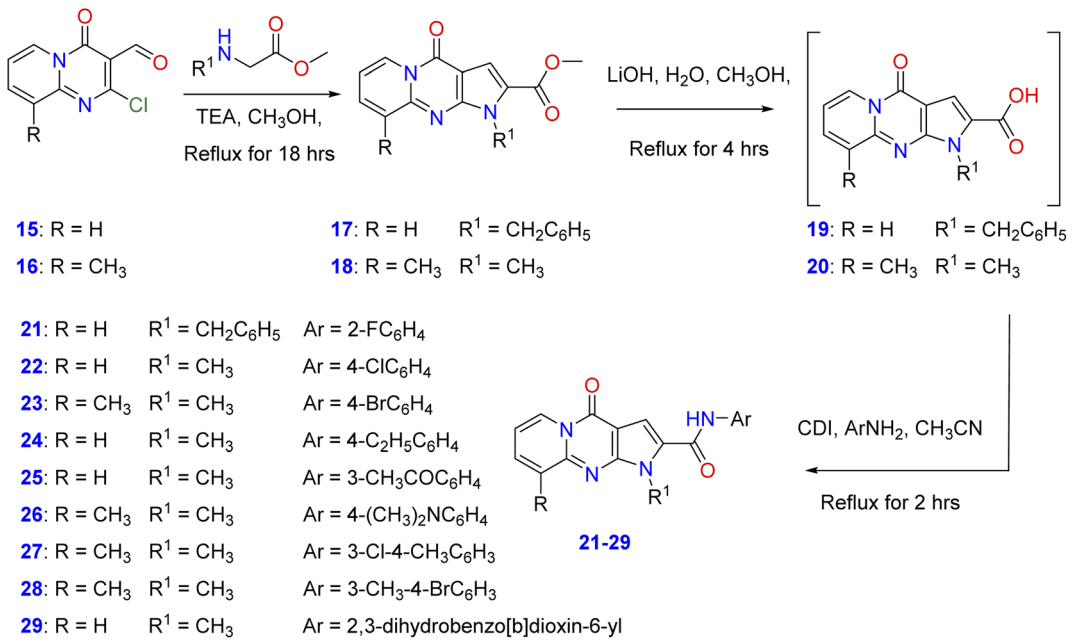

Scheme 1 Synthetic protocol of pyrido[1,2-*a*]pyrrolo[2,3-*d*]pyrimidine derivatives (**21–29**).

Table 1 Antiviral activity and cytotoxicity assay of novel non-covalent SARS-CoV-2 M^{pro} inhibitors by propagation in Vero E6 cells

		Antiviral assay (qPCR)				
		Inhibition %		EC_{50} and EC_{90} ($\mu M \pm SE^a$)		
Comp. ID	Cytotoxicity IC_{50} ($\mu M \pm SE^a$)	1 μM	10 μM	EC_{50}	EC_{90}	SI^b
17	>200	22.25	42.51	22.1 ± 1.012	36.13 ± 2.31	9
21	48.8 ± 3.72	83.49	95.92	0.0138 ± 0.00198	3.60 ± 0.42	3544
22	193.0 ± 14.7	88.16	94.10	0.1093 ± 0.01105	1.738 ± 0.54	1766
23	47.6 ± 3.62	78.96	92.92	0.0216 ± 0.00656	3.11 ± 1.61	2201
24	21.6 ± 1.64	94.01	96.22	0.0762 ± 0.00973	3.437 ± 0.55	283.3
25	121.0 ± 9.21	92.48	97.08	0.1066 ± 0.00115	2.50 ± 0.841	1135
26	87.3 ± 6.65	87.61	94.05	0.0376 ± 0.00423	3.801 ± 0.041	2323
27	64.4 ± 4.91	94.36	96.52	0.1035 ± 0.00344	2.601 ± 1.02	622.2
28	139.0 ± 10.6	92.71	95.60	0.108 ± 0.00304	1.41 ± 0.91	1278
29	151.0 ± 11.5	94.10	96.39	0.0519 ± 0.00512	8.953 ± 2.01	2909
Remdesivir	43.1 ± 3.28	94.23	97.58	0.0099 ± 0.00175	0.0835 ± 1.88	7195

[a] SE represents standard error from triplicate readings. [b] Selectivity index (SI) was calculated by dividing of IC_{50} value for Vero cell cytotoxicity by the EC_{50} of the antiviral assay.

addition, cell growth inhibition or cytotoxicity was determined for all analogs (**17**, and **21–29**) and remdesivir as a positive control. All the obtained data are presented in Table 1. It was found that remdesivir showed potent antiviral activity EC_{50} = 0.0099 μM with prominent cytotoxicity to Vero E6 cells with an IC_{50} value of 43.1 μM and SI index of 1481. As a preliminary evaluation step for the precursor compound **17** with ester group; it has no cytotoxic effect with weak antiviral activity compared to the target compounds by EC_{50} = 22.1 μM. Thus, the chemical modification of such compound into **21–29** substituted amides revealed a good effect on the antiviral activity profile with an acceptable MTT cytotoxicity effect. Moreover, all tested compounds showed cytotoxicity with IC_{50} values over that of remdesivir except for **24** which showed the highest cytotoxicity equal to 21.60 ± 1.64 μM with good M^{pro} inhibitory activity. The pyridopyrrolopyrimidine derivatives **22**, **29**, and **28** showed the lowest MTT IC_{50} cytotoxicity (193.0, 151.0, and 139.0) with EC_{50} values of 0.109, 0.051, and 0.108 μM towards the infected Vero cells. Interestingly, analog **29** with benzodioxan terminal part had a potent antiviral profile with percent inhibition values of 94.10 and 96.39% at 1 and 10 micromolar concentrations, respectively which were found to be very close to results of the positive control remdesivir (94.23 and 97.58%) at the same concentrations. The benzodioxan derivative was found to have the preferential of the lowest cytotoxic action (IC_{50} = 151.00 μM). In addition, **26**, **21**, and **23** analogs exhibited promising antiviral effects with percent inhibition values of 94.50, 95.92, and 92.92% at 10 μM, respectively. The problem with **21** and **23** is their elevated cytotoxic tendency to Vero cells.

The selectivity analysis of these compounds compared to their cytotoxic effect has also been investigated. Good antiviral candidate should be highly selective with a minimum SI value of 5 or higher.[36–39] Almost all the new pyridopyrrolopyrimidines showed good SI values and proved the prominent antiviral activity. Comparing the performance of novel compounds to the reference remdesivir, SI was calculated and showed 4000 to 283 ranges with promising antiviral selectivity. Some of the designed derivatives did not function positively in the antiviral activity *in vitro*, and their relative abilities to inhibit viral replication did not always correlate directly with *in vitro* inhibition parameters toward M^{pro}.[40]

SARS-CoV-2 M^{pro} inhibition assay. Both the crystal structures of human coronavirus M^{pro} and for an inhibitor complex of porcine coronavirus M^{pro} were determined and led to a construction of a homology model for SARS-CoV-2-M^{Pro}.[16] The main protease, M^{pro} in SARS-CoV-2 is considered a viable drug target because of its important role in the cleavage of the virus polypeptide.[41–43] Several M^{pro} inhibitors have been reported as covalent or non-covalent inhibitors. The covalent inhibitors work by modifying the catalytic Cys145 with potent enzymatic inhibition and cellular antiviral activity, including GC376, PX-12, and carmofur, each containing a reactive nitrogen heterocycle as pyrrolidone, imidazole, or pyrimidine that mimics the glutamine P1 position.[44–46] Interestingly, many non-covalent inhibitors of SARS-CoV-2 M^{pro} were developed and validated such as ML188.[47]

Herein, *N*-aryl-1-benzyl/methyl-4-oxo-1,4-dihydropyrido[1,2-*a*]pyrrolo[2,3-*d*]pyrimidine-2-carboxamide derivatives were tested by *in vitro* assay for inhibition of SARS-CoV-2 M^{pro} activity and compared with the known references Lopinavir (non-specific) and GC376 (specific) M^{pro} inhibitors.[48] As shown in Table 2, intermediate **17** seems to be functionally inactive against the M^{pro} enzyme as seen from its IC_{50} value. However, both **25** and **29**exhibited high SARS-CoV-2 M^{pro} inhibition activity with IC_{50} values of 5.42 and 3.22 μM, respectively, which are more potent than the reference drugs Lopinavir and GC376 (82.17, 12.85 μM). On the other hand, introducing a halogen substituent to the terminal aryl ring, as in cases of **27**, **28**, **23** and **22**, leads to a dramatical fall in the activity (IC_{50} values = 165.20 μM, 45.96 μM, 65.92 μM and 236.50 μM, respectively). As well, compound **26** with *N*,*N*-dimethylamino group at the *para* position of the terminal aryl showed a dramatic reduction in the inhibition activity with (IC_{50} values 407.50 μM). In combination

Table 2 Inhibitory data of the target compounds against SARS-CoV-2 M^{pro}

Compound's ID	IC_{50} (μM ± SE[a])	Compound's ID	IC_{50} (μM ± SE[*])
17	329.5 ± 15.1	**26**	407.50 ± 3.44
21	25.36 ± 2.40	**27**	165.20 ± 16.70
22	236.50 ± 4.29	**28**	45.96 ± 8.62
23	65.92 ± 12.30	**29**	3.22 ± 2.83
24	82.17 ± 15.0	**Lopinavir**	82.17 ± 7.66
25	5.42 ± 21.30	**GC-376**	12.85 ± 0.74

[a] SE represents standard deviation from triplicate readings.

with results presented in Table 1, this indicates that the 3,4-dihydrodioxane or 3-acetyl group attached to the phenyl ring is necessary for activity against M^{pro} of these compounds. The results all partially conveyed the proposed inhibitory effect of these derivatives on the M^{pro}, but more mechanistic investigations are still needed to specify the major mechanism of action whether it is competitive on non-competitive.

SAR analysis. The antiviral assay results indicated that the target compounds showed excellent antiviral activity against SARS-CoV-2-M^{Pro}. Results in Table 2 showed that when the aryl substituent is 3,4-dihydrobenzo[*b*]dioxin-6-y (**29**), 3-acetylC_6H_4 (**25**) groups, on the corresponding target compounds, it exhibited good protection activity. Moreover, the results showed that the increase in the hydrogen bond accepter and hydrophobicity increases the interaction within pocket and consequently improves the activity. Steric hindrance effect on aromatic rings in the pocket well decrease activity for antiviral activity at the same position confirmed by the following activity order; **26** (Ar = 4-*N*,*N*-dimethyl-Ph) > **22** (Ar = 4-Cl-Ph) > **27** (Ar = 3-Cl-4-CH_3-Ph) > **24** (Ar = 4-C_2H_6-Ph) > **23** (Ar = 4-Br-Ph) > **28** (Ar = 3-CH_3, 4-Br-Ph), > **21** (Ar = 2-F-Ph). The activity of these analogs could be attributed in general to the 5-membered aromatic pyrrole ring which correctly and precisely orients the amide bond to the molecule within the binding site. A summary of the SAR analysis is presented in Fig. 4.

Computational investigations

Molecular docking study. To gain better understanding on the potency of the studied compound, to explicate the plausible mechanism by which it can induce antiviral activity and guide further SAR studies, we proceeded to examine the interaction of the most active pyrido[1,2-*a*]pyrrolo[2,3-*d*]pyrimidine derivative (**29**) with SARS-CoV-2 M^{pro} protein. Here, the structure of SARS-CoV-2 M^{pro} in complex with a potent bipyridine-benzonitrile inhibitor (**XF1**) crystal structure (PDB: 7L11) was selected as the binding model.[49] This molecular docking study was performed using the default protocol associated with the glide module of the Schrodinger modelling suite.[50–52] Results showed that compound **29** was appropriately oriented in the active site of SARS-CoV-2 M^{pro} protein with a significant docking score (−7.45 kcal Mol^{-1}) and displayed three hydrogen binding interactions with amino acids Gly143, Cys145, and Glu166 as depicted in Fig. 5A and B. The co-crystallized ligand exhibited two hydrogen binding interactions with the first couple of amino acids while the third one interacted hydrophobically with XF1. The binding affinity exhibited by compound **29** is attributed to significant bonded and non-bonded interactions with residues lining the active site of the SARS-CoV-2 M^{pro} which is supported by the following finding: an arene–arene interaction with catalytic residue His41; hydrogen bond interaction between amide carbonyl and the NH of Cys145; as well as the hydrogen bond interaction between the carbonyl of the fused system with Glu166. An additional bi-directional hydrophobic interaction arose between both six-membered rings of the new pyridopyrrolopyrimidine-2-carboxamide with the crucial amino acid residue Met165. The binding pocket per residue interaction analysis for the active compound **29** showed that the molecule is embedded into the active site through a series of significant van der Waals interactions (Table 3). Docking score of the compound **29** was close to those of Co-Crystalized ligand (−10.07 kcal mol^{-1}) showing that this compound may bind to SARS-CoV-2 M^{pro} catalytic site with good affinity. To validate results of our conducted docking experiment, we a used docking control in which the internal co-crystallized ligand **XF1** was re-docked into the binding pocket of the chosen crystal structure. Results of this validation process revealed an acceptable superimposition of the re-docked **XF1** conformer over that of the crystal structure and showed a RMSD value of 1.49 (Fig. S1; see ESI†). As well, a set of almost matching hydrogen bonding and hydrophobic interactions with that observed in the case of compound **29** was obtained (Fig. 5C and D).

Molecular dynamic (MD) simulation. MD simulations can be used to determine the dynamic and thermodynamic parameters of living systems under specific conditions of physiological

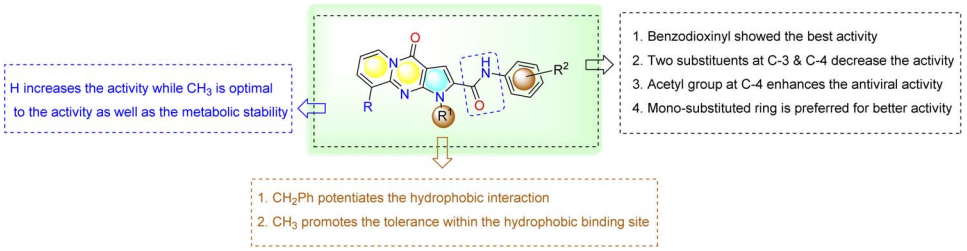

Fig. 4 SAR analysis of target compounds correlated with M^{pro} protease activity.

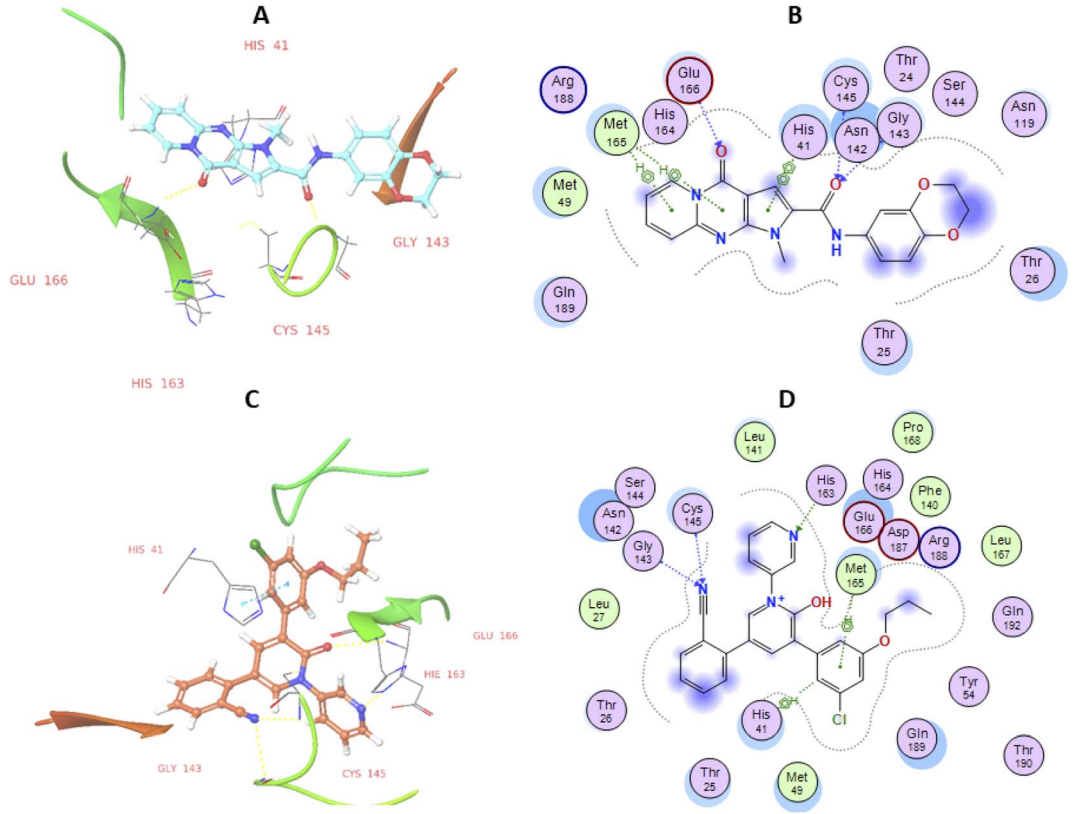

Fig. 5 2D and 3D binding interaction data of active **29** analog (A and B) compared to Co-Crystalized ligand (C and D) in active site of SARS-CoV 2 M^{pro} enzyme with PDB entry code 7L11. Color-coding scheme for interaction includes polar hydrogen bonding interaction as blue or green arrows and non-polar aromatic type as green lines mediated with small aromatic ring.

Table 3 Comparative analysis of interaction data of **29** and reference bound compounds

		Binding pocket residue interaction									
		His41		Cys145		Gly143		His163		Glu166	
IDs	Score	VWD[a]	*D*	VWD	*D*	VWD	*D*	VWD	*D*	VWD	*D*
29	−7.45	−3.86	2.23	−2.81	3.44	−2.48	2.11	−0.44	4.88	−2.57	2.16
Ref.	−10.1	−4.71	3.01	−3.47	2.32	−1.66	2.61	−1.11	2.02	−4.85	2.17

[a] VWD = van der Waals interactions (kcal mol^{-1}) *D* = Distance (Å).

environments,[53,54] which is very computationally demanding process, hence we used MD simulations to explore the binding stability and conformational behavior of the **29** SARS-CoV-2 M^{pro} complex in physiological environments through time. The MD simulation of 100 ns time in an explicit solvent system was performed using the Desmond software. The simulated complexes' trajectories were examined for various conventional simulation parameters, such as backbone root-mean standard deviations (RMSD) for α-carbon atoms. Furthermore, the root-mean square fluctuations (RMSF) of particular amino acid residues, as well as ligand protein contact mapping, were assessed. A lower RMSD value throughout the MD simulation indicates the protein–ligand complex is more stable, whereas a higher RMSD value reveals that the protein–ligand complex is less stable. Fig. 6B shows the RMSD of the Cα backbone (blue) of SARS-CoV-2 M^{pro} protein throughout the simulation based on the reference frame backbone. The maximum RMSD value of Cα backbone of SARS-CoV-2 M^{pro} protein is 2.7 Å, which indicates that the **29**–SARS-CoV-2 M^{pro} complex was retained consistently during the simulation time.

After the early fluctuation due to the equilibration, the RMSD of the compound **29** remained constant with 3.5 Å till 55 ns, after which minor RMSD fluctuation was noticed and remained stable for the rest of the simulation. The mobility of amino acid residues was assessed throughout time simulation using the protein RMSF in comparison to a reference structure. In the protein RMSF plot, α-helical and β-strand regions are represented in red and blue colors, respectively, while in the white

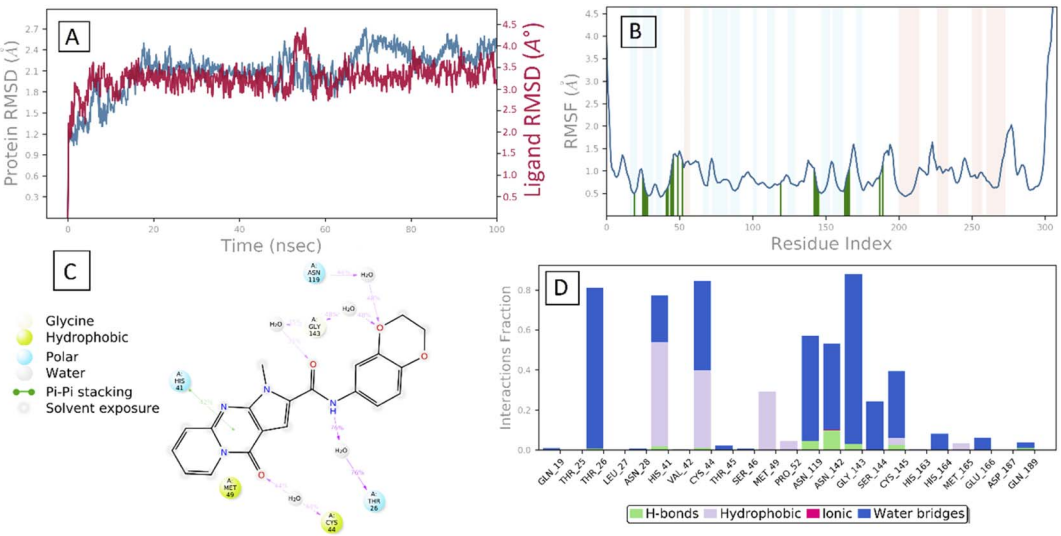

Fig. 6 MD simulation analysis of **29**–SARS-CoV-2 M^{pro} (A) RMSD (Protein RMSD is presented in grey while RMSD of compound **29** are presented in red color) (B) protein amino acids RMSF (C) 2D ligand interaction diagram and (D) protein–ligand contact analysis of MD trajectory.

color, the loop region is represented. Protein α-helical and β-strands regions are stiffer than the unstructured region of protein and as a result, fluctuate less than loop regions. If the active site and main chain atoms fluctuated insignificantly, it indicated that the conformational change was minimal, implying that the reported lead compound was tightly bound within the cavity of the SARS-CoV-2 M^{pro} protein binding pocket. The RMSF plot of **29**–SARS-CoV-2 M^{pro} is displayed in Fig. 3B. According to the RMSF plot, it was observed that compound **29** contacted 23 amino acids of SARS-CoV-2 M^{pro} binding pocket, namely, Gln19, Thr25, Thr26, Leu27, Asn28, His41, Val42, Cys44, Thr45, Ser46, Met49, Pro52, Asn119, Asn142, Gly143, Ser144, Cys145, His163, His164, Met165, Glu166, Asp187, and Gln189. All this interacted residue is marked in green-colored vertical bars, having a RMSF value of less than 1.5 Å. Compound **29** was able to tightly bind to the active site through multiple interactions, including 42% simulation time of π–π stacking with catalytic dyed residue His 41 (Fig. 6C). Fig. 3D indicates that Compound **29** forms hydrophobic and water mediated hydrogen bonding with Tyr25, Asn28, Cys44, Met49, Asn119, Asn142, Gly143, Ser144 and Cys145. It visible that compound **29** made all three types (hydrogen, hydrophobic and water mediated hydrogen bonding) of interaction with crucial residues His 41 and Cys145. All the amino acid interactions identified during docking studies of the target molecule were also displayed during the dynamic study.

Conclusion

In conclusion, we have designed a new set of novel pyrido[1,2-*a*]pyrrolo[2,3-*d*]pyrimidine-2-carboxamides and evaluated their antiviral activity against COVID-19. Most of the designed compounds exhibited potent antiviral activity. SAR analysis of the novel scaffold was estimated based on biological and theoretical results obtained for these compounds. The benzodioxan derivative **29** showed very potent anti-SARS-CoV-2 activity at the concentrations of 1 and 10 μM by 94.10 and 96.39% inhibition of the viral growth with $EC_{50} = 0.0519$ μM. These novel derivatives were subjected to M^{pro} protease inhibitory assay and molecular docking study to better understand their underlying mechanism. Compound **29** strongly inhibited the activity of M^{pro} with an IC_{50} value of 3.22 μM compared to 12.85 μM for the reference control GC-376. Results of molecular docking study exhibited that compound **29** works through the non-covalent interaction with the main protease of SARS-CoV. Also, a molecular dynamic simulation study has been performed. Docking and dynamic simulations studies proved the prominent interaction behaviour and stability of **29** within the binding pocket through the conserved His41, Glu166, and Cys145 residues. More mechanistic investigations are still needed to decide whether this compound is a competitive or non-competitive inhibitor of the SARS-CoV M^{pro}.

Materials and method

General

All chemicals were purchased from Sigma-Aldrich Chemical Co. (Sigma-Aldrich Corp., St. Louis, MO, USA). All the melting points were measured with a Stuart Scientific Co. Ltd apparatus, which are uncorrected. The ^1H (500 MHz) NMR spectra were measured on a BRUKER AV 500 MHz spectrometer in DMSO-d_6, a solvent, using the tetramethylsilane (TMS) as an internal standard. The mass spectra were determined on Agilent 1100 LC MSD Model G1315B Mass Spectrometer (Agilent Technologies, United States). The elemental analysis was carried out at the Regional Centre for Mycology and Biotechnology (RCMP), Al-Azhar University, Cairo, Egypt, and the results were within ± 0.25%. The reaction courses and product mixtures were routinely monitored by the thin layer chromatography (TLC) on silica gel pre-coated F_{254} Merck plates.

General procedure for synthesis of methyl 1-benzyl/methyl-4-oxo-1,4-dihydropyrido[1,2-*a*]pyrrolo[2,3-*d*]pyrimidine-2-carboxylate and 9-methyl derivative (17, 18)

A reaction mixture of 2-chloro-4-oxo-4*H*-pyrido[1,2-*a*]pyrimidine-3-carbaldehyde or its 9-methyl derivative (**15, 16**) (0.01 mol)[55] with methyl-*N*-methyl(*N*-benzyl)glycinate or methyl methyl-*N*-benzyl glycinate (0.01 mol) in methanol (20 ml) and triethylamine (0.5 ml) was heated under reflux conditions for 4 h. After the reaction reached completion, the reaction mixture was cooled to room temperature, and the precipitated solid was filtered off, washed with cold methanol, and recrystallized from ethanol/benzene to give compounds **17** and **18** are as previously described.[12]

General procedure for synthesis of 1-benzyl/methyl-4-oxo-1,4-dihydropyrido[1,2-*a*]pyrrolo[2,3-*d*]pyrimidine-2-carboxylic acid (19, 20) and *N*-aryl-1-benzyl/methyl-4-oxo-1,4-dihydropyrido[1,2-*a*]pyrrolo[2,3-d]pyrimidine-2-carboxamide (21–29)

A reaction mixture of methyl 1-benzyl/methyl-4-oxo-1,4-dihydropyrido[1,2-*a*]pyrrolo[2,3-*d*]-pyrimidine-2-carboxylate or its 9-methyl derivatives (**17, 18**) (0.01 mol) in aq. lithium hydroxide (0.01 mol) in methanol (20 ml) was refluxed for 2 h. After the reaction reached completion, the reaction mixture was cooled to room temperature, andthe methanol was removed under reduced pressure till dryness, the obtained oil intermediate, 1-benzyl/methyl-4-oxo-1,4-dihydropyrido[1,2-*a*]pyrrolo[2,3-*d*] pyrimidine-2-carboxylic acid or its 9-methyl derivatives (**19, 20**) was then washed with 10% HCl then H_2O and the remaining oil was extracted by acetonitrile. The latter was reacted withvarious aromatic amines (0.01 mol) in the presence of 1,1′-carbonyldiimidazole (CDI) (0.01 mol) and acetonitrile (20 ml) under reflux for 4 h. The resultant precipitates were filtered off and the filtrate was evaporated to dryness. The residue was subjected to a column chromatography on silica gel with hexane/ethyl acetate (EtOAc) (3 : 1) as an eluent to afford the target *N*-aryl-1-benzyl/methyl-4-oxo-1,4-dihydropyrido[1,2-*a*]pyrrolo[2,3-*d*] pyrimidine-2-carboxamide (**21–29**). The physical and spectral data of compounds (**21–29**) are as follows:

1-Benzyl-*N*-(2-fluorophenyl)-4-oxo-1,4-dihydropyrido[1,2-*a*] pyrrolo[2,3-*d*]pyrimidine-2-carboxamide (21). Colorless needles from ethanol/benzene; yield 87%; mp. 215–217 °C; ^{1}H NMR (DMSO-d_6, 400 MHz) δ: 10.14 (bs, 1H, NH), 8.97, 8.94 (d, 1H, J = 11.6 Hz, pyridine, H-6), 7.78 (s, 2H, Ar, H-3,5), 7.62, 7.60 (d, 1H, J = 9.2 Hz, pyridine, H-8), 7.52 (t, 1H, J = 7.6 Hz, pyridine, H-7), 7.31–7.15 (m, 9H, pyridine H-9, pyrrole H-3 and Ar-H), 5.88 (s, 2H, CH_2); ^{13}C NMR (DMSO-d_6) δ: 168.72 (CO), 165.72 (CO), 161.72 (C-10a), 159.79 (C-2, Ph), 158.00 (C-9a), 151.94 (C-1, $PhCH_2$), 147.21 (C-8), 143.94 (C-1, Ph), 141.94 (C-4, Ph), 131.58 (C-3,5, Ph), 130.00 (C-2,6, Ph), 129.04 (C-6), 128.97 (C-2), 125.99 (C-4, $PhCH_2$), 120.42 (C-9, C-6, Ph), 116.84 (C-3), 115.43 (C-3, Ph), 115.25 (C-7), 114.04 (C-1, Ph), 103.16 (C-3a), 55.11 (CH_2); LCMS (electrospray) m/z (M^+ + 1) 413; Anal. Calcd for $C_{24}H_{17}FN_4O_2$ (412.42): C, 69.89; H, 4.15; N, 13.59. Found: C, 69.95; H, 4.19; N, 13.63%.

***N*-(4-Chlorophenyl)-1-methyl-4-oxo-1,4-dihydropyrido[1,2-*a*] pyrrolo[2,3-*d*]pyrimidine-2-carboxamide (22).** Colorless needles from ethanol/benzene; yield 89%; mp. 245–247 °C; ^{1}H NMR (DMSO-d_6, 400 MHz) δ: 10.18 (bs, 1H, NH), 8.93, 8.91 (d, 1H, J = 8 Hz, pyridine, H-6), 8.83, 8.81 (d, 2H, J = 8 Hz, Ar-H-2,6), 7.73 (s, 1H, pyrrole, H-3), 7.70, 7.86 (d, 1H, J = 8 Hz, pyridine, H-8), 7.54, 7.52 (d, 1H, J = 8 Hz, pyridine, H-9), 7.30, 7.28 (d, 2H, J = 8 Hz, Ar-H-3,5), 7.06 (t, 1H, J = 8 Hz pyridine, H-7), 4.09 (s, 3H, CH_3); ^{13}C NMR (DMSO-d_6) δ: 169.74 (CO), 168.17 (CO), 162.74 (C-10a), 160.17 (C-9a), 147.24 (C-1, Ph), 144.70 (C-8), 131.56 (C-4, Ph), 131.11 (C-3,5, Ph), 130.03 (C-6), 129.32 (C-2), 128.60, 128.29 (C-2,6, Ph), 125.97 (C-9), 120.37 (C-3), 114.40 (C-7), 103.11 (C-3a), 37.32 (CH_3); LCMS (electrospray) m/z (M^+ + 1) 353, m/z (M^+ + 3) 355; Anal. Calcd for $C_{24}H_{17}ClN_4O_2$ (352.77): C, 61.28; H, 3.71; N, 15.88. Found: C, 61.21; H, 3.65; N, 15.83%.

***N*-(4-Bromophenyl)-1-methyl-4-oxo-1,4-dihydropyrido[1,2-*a*] pyrrolo[2,3-*d*]pyrimidine-2-carboxamide (23).** Colorless needles from ethanol/benzene; yield 86%; mp. 278–280 °C; ^{1}H NMR (DMSO-d_6, 400 MHz) δ: 10.32 (bs, 1H, NH), 8.83, 8.81 (d, 1H, J = 7.6 Hz, pyridine, H-6), 7.77, 7.75 (d, 2H, J = 6 Hz, Ar-H-2,6), 7.71 (s, 1H, pyrrole, H-3), 7.66, 7.65 (d, 2H, J = 8.4 Hz, Ar-H-3,5), 7.54, 7.51 (d, 1H, J = 8.8 Hz, pyridine, H-8), 7.02 (t, 1H, J = 12 Hz pyridine, H-7), 4.02 (s, 3H, CH_3), 2.25 (s, 3H, CH_3); ^{13}C NMR (DMSO-d_6) δ: 168.68 (CO), 165.04 (CO), 160.24 (C-10a), 147.24 (C-9a), 145.12 (C-1, Ph), 131.55 (C-8), 131.52 (C-3,5, Ph), 130.05 (C-6), 129.39 (C-2), 128.28 (C-9), 125.97 (C-2,6, Ph), 120.37 (C-4, Ph), 119.61 (C-3), 114.05 (C-7), 103.11 (C-3a), 37.39 (CH_3); LCMS (electrospray) m/z (M^+ + 1) 413, m/z (M^+ + 3) 415; Anal. Calcd for $C_{24}H_{17}BrN_4O_2$ (411.25): C, 55.49; H, 3.68; N, 13.62. Found: C, 55.43; H, 3.61; N, 13.57%.

***N*-(4-Ethylphenyl)-1-methyl-4-oxo-1,4-dihydropyrido[1,2-*a*] pyrrolo[2,3-*d*]pyrimidine-2-carboxamide (24).** Colorless needles from ethanol/benzene; yield 86%; mp. 260–262 °C; ^{1}H NMR (DMSO-d_6, 400 MHz) δ: 10.18 (bs, 1H, NH), 8.91, 8.89 (d, 1H, J = 8.0 Hz, pyridine, H-6), 7.78, 7.76 (d, 2H, J = 8.0 Hz, Ar-H-2,6), 7.76 (s, 1H, pyrrole, H-3), 7.68, 7.66 (d, 2H, J = 8.0 Hz, Ar-H-3,5), 7.59, 7.57 (d, 1H, J = 8.0 Hz, pyridine, H-8), 7.19, 7.17 (d, 1H, J = 8.0 Hz, pyridine, H-9), 7.12 (t, 1H, J = 8.0 Hz pyridine, H-7), 4.01 (s, 3H, CH_3), 2.58 (q, 2H, J = 8.0, CH_2), 1.71 (s, 3H, J = 8.0, CH_3); LCMS (electrospray) m/z (M^+ + 1) 347; Anal. Calcd for $C_{20}H_{18}N_4O_2$ (346.38): C, 69.35; H, 5.24; N, 16.17. Found: C, 69.29; H, 5.19; N, 16.11%.

***N*-(3-Acetylphenyl)-1-methyl-4-oxo-1,4-dihydropyrido[1,2-*a*] pyrrolo[2,3-*d*]pyrimidine-2-carboxamide (25).** Yellow needles from ethanol/benzene; yield 81%; mp. 238–240 °C; ^{1}H NMR (DMSO-d_6, 400 MHz) δ: 10.41 (bs, 1H, NH), 8.94, 8.92 (d, 1H, J = 8.0 Hz, pyridine, H-6), 8.38 (s, 1H, Ar-H-2), 8.08, 8.06 (d, 1H, J = 8.4 Hz, pyridine, H-8), 7.77 (s, 1H, pyrrole, H-3), 7.72, 7.70 (d, 1H, J = 8.0 Hz, Ar-H-6), 7.61, 7.59 (d, 1H, J = 8.0 Hz, Ar-H-4, pyridine, H-9), 7.51 (t, 1H, J = 8.0 Hz, Ar-H-5), 7.13 (t, 1H, J = 7.2 Hz pyridine, H-7), 4.03 (s, 3H, CH_3), 2.59 (s, 3H, $COCH_3$); LCMS (electrospray) m/z (M^+) 360; Anal. Calcd for $C_{20}H_{16}N_4O_3$ (360.37): C, 66.66; H, 4.48; N, 15.55. Found: C, 66.61; H, 4.44; N, 15.50%.

***N*-(4-(Dimethylamino)phenyl)-1,9-dimethyl-4-oxo-1,4-dihydropyrido[1,2-*a*]pyrrolo[2,3-*d*]-pyrimidine-2-carboxamide (26).** Yellow needles from ethanol/benzene; yield 81%; mp. 267–269 °C; ^{1}H NMR (DMSO-d_6, 400 MHz) δ: 9.99 (bs, 1H, NH), 8.82, 8.80 (d, 1H, J = 8.0 Hz, pyridine, H-6), 7.63, 7.61 (d, 2H, J =

8.0 Hz, Ar-H-2,6), 7.60 (s, 1H, pyrrole, H-3), 7.60,7.57 (d, 1H, J = 12.0 Hz, pyridine, H-8), 7.00 (t, 1H, J = 12 Hz pyridine, H-7), 6.75, 6.73 (d, 2H, J = 8.0 Hz, Ar-H-3,5), 4.01 (s, 3H, CH_3), 2.85 [s, 6H, $N(CH_3)_2$], 2.50 (s, 3H, CH_3); ^{13}C NMR (DMSO-d_6) δ: 168.68 (CO), 165.04 (CO), 160.24 (C-10a), 147.24 (C-9a), 145.12 (C-1, Ph), 131.55 (C-8), 131.52 (C-3,5, Ph), 130.05 (C-6), 129.39 (C-2), 128.28 (C-9), 125.97 (C-2,6, Ph), 120.37 (C-4, Ph), 119.61 (C-3), 114.05 (C-7), 103.11 (C-3a), 37.39 (CH_3); LCMS (electrospray) m/z (M^+ + 1) 376, (M^+ + 2) 377; Anal. Calcd for $C_{21}H_{21}N_5O_2$ (375.42): C, 67.18; H, 5.64; N, 18.65. Found: C, 67.24; H, 5.69; N, 18.70%.

***N*-(3-Chloro-4-methylphenyl)-1,9-dimethyl-4-oxo-1,4-dihydropyrido[1,2-*a*]pyrrolo[2,3-*d*]-pyrimidine-2-carboxamide (27).** Pale yellow needles from ethanol/benzene; yield 81%; mp. 280–282 °C; ^{1}H NMR (DMSO-d_6, 400 MHz) δ: 10.22 (bs, 1H, NH), 8.83, 8.81 (d, 1H, J = 7.2 Hz, pyridine, H-6), 7.79 (s, 1H, Ar, H-2), 7.70 (s, 1H, pyrrole, H-3), 7.66, 7.64 (s, 1H, J = 8.0 Hz, Ar, H-6), 7.57, 7.55 (s, 1H, J = 8.4 Hz, Ar, H-5), 7.52,7.50 (d, 1H, J = 8.4 Hz, pyridine, H-8), 7.03 (t, 1H, J = 7.6 Hz pyridine, H-7), 4.02 (s, 3H, CH_3), 2.50 (s, 3H, CH_3), 2.29 (s, 3H, CH_3); LCMS (electrospray) m/z (M^+) 381, (M^+ + 2) 383, (M^+ + 3) 384; Anal. Calcd for $C_{20}H_{17}ClN_4O_2$ (380.83): C, 63.08; 4.50; N; 14.71. Found: C, 63.01; 4.44; N; 14.67%.

***N*-(4-Bromo-3-methylphenyl)-1,9-dimethyl-4-oxo-1,4-dihydropyrido[1,2-*a*]pyrrolo[2,3-*d*]-pyrimidine-2-carboxamide (28).** Yellow needles from ethanol/benzene; yield 82%; mp. 230–232 °C; ^{1}H NMR (DMSO-d_6, 400 MHz) δ: 10.22 (bs, 1H, NH), 8.83, 8.81 (d, 1H, J = 7.2 Hz, pyridine, H-6), 7.79 (s, 1H, Ar, H-2), 7.03 (s, 1H, pyrrole, H-3), 7.66, 7.64 (s, 1H, J = 8.0 Hz, Ar, H-6), 7.57, 7.55 (s, 1H, J = 8.4 Hz, Ar, H-5), 7.52,7.51 (d, 1H, J = 6.4 Hz, pyridine, H-8), 7.03 (t, 1H, J = 7.6 Hz pyridine, H-7), 4.02 (s, 3H, CH_3), 2.52 (s, 3H, CH_3), 2.34 (s, 3H, CH_3); LCMS (electrospray) m/z (M) 424, (M++1) 425, (M++4) + 428; Anal. Calcd for $C_{20}H_{17}BrN_4O_2$ (425.28): C, 56.48; H, 4.03; N; 13.17. Found: C, 56.41; H, 4.00; N; 13.12%.

***N*-(2,3-Dihydrobenzo[*b*][1,4]dioxin-6-yl)-1-methyl-4-oxo-1,4-dihydropyrido[1,2-*a*]pyrrolo-[2,3-*d*]pyrimidine-2-carboxamide (29).** Pale yellow needles from ethanol/benzene; yield 81%; mp. 215–217 °C; ^{1}H NMR (DMSO-d_6, 400 MHz) δ: 10.08 (bs, 1H, NH), 8.94, 8.92 (d, 1H, J = 8.0 Hz, pyridine, H-6), 8.80 (s, 1H, Ar-H-2), 7.76, 7.74 (d, 1H, J = 8.0 Hz, pyridine, H-8), 7.65 (s, 1H, pyrrole, H-3), 7.61, 7.59 (d, 1H, J = 8.0 Hz, Ar-H-9), 7.21, 7.19 (d, 1H, J = 8.8 Hz, Ar-H-6), 7.12 (t, 1H, J = 8.0 Hz pyridine, H-7), 6.84, 6.81 (t, 1H, J = 8.8 Hz, Ar-H-5), 4.33 (s, 4H, $2CH_2$), 4.03 (s, 3H, CH_3); LCMS (electrospray) m/z (M^+ + 1)377; Anal. Calcd for $C_{20}H_{16}N_4O_3$ (376.37): C, 63.82; H, 4.28; N, 14.89. Found: C, 63.88; H, 4.34; N, 14.94%.

Biological evaluation studies

Antiviral assay. To determine the effect of target compounds on SARS-CoV-2 viral load (SARS-CoV-2 isolate EGY/WAT-2 VACCERA), qualitative detection of SARS-CoV-2 viral RNA was carried out using a Real-Time PCR assay.[56] Total RNA was extracted using genesig® Coronavirus SARS-CoV-2 Real-Time PCR Assay kit (Primer design TM Ltd, Southampton, United Kingdom) according to the manufacturer's protocol.[57] Briefly, a monolayer of Vero cells was prepared in a 96-well plate. The cells were then treated with a single non-toxic dose of each compound in a triplicate and infected with SARS-CoV-2 at a MOI of 0.01 with incubation period of 1 h at 37 °C followed by removal of inoculum and overlaying with cell culture media containing the test compound. As a vehicle control, cells in three wells were treated with 0.1% DMSO diluted with cell culture media. The plate was kept for 48 h at 37 °C in the presence of 5% CO_2, followed by performing a virus yield inhibition assay using qRT-PCR on harvested supernatants from the wells. This kit contains a master mix, primers, and probe designed for reverse transcription of the extracted RNA and Real-Time PCR for the detection of SARS-CoV-2. The assay was performed using the Rotor-Gene Q instrument (Qiagen, Germany) under the following amplification conditions: 10 min Reverse Transcription at 55 °C, 2 min initial activation at 95 °C, followed by 45 cycles of 10 s denaturation at 95 °C and 60 s annealing and extension at 60 °C (see ESI†). The target compounds were further assessed using a dose response assay by adding to cells at five different concentrations of 10, 1, 0.1, 0.01, and 0.001 μM. EC_{50} and EC_{90} values that produce virus-induced cell death were measured. Selectivity index (SI) was calculated as a ratio of drug's IC_{50} and EC_{50} values (SI = IC_{50}/EC_{50}).

Cytotoxicity evaluation using a viability assay. The cytotoxic activity was assessed using the MTT colorimetric assay as reported previously.[58–62] In brief, tumour cell lines were suspended in medium at concentration 5 × 10^4 cell/well in Corning® 96-well tissue culture plates and then incubated for 24 h. The tested compounds with concentrations ranging from 0 to 50 μg ml^{-1} were then added into 96-well plates (in a triplicate) to achieve different concentrations for each compound. Vehicle controls with media or 0.5% DMSO were run for each 96 well plate as a negative control. After incubating for 24 h, the numbers of viable cells were determined.

SARS-CoV-2-M^{Pro} inhibition assay. Kits of SARS-CoV-2 M^{pro} with an internally quenched substrate, and assay buffer were purchased from BPS Bioscience (San Diego, CA, USA). The SARS-CoV-2-M^{Pro} enzyme assay was developed in 384-well black, medium binding microplates with a total volume of 20 μL and then reduced to 1536-well format as previously reported.[63] In a 384-well plate format, 10 μL of SARS-CoV-2 M^{pro} in reaction buffer was added into each well, followed by the addition of 10 μL of the inhibitor compound.[63,64] Fluorescent intensity was measured at different time intervals. Briefly, 10 μl of drugs (250 μM) were incubated for 1 hour with 4 ng M^{pro}-MBP tagged enzyme in 30 μl of assay buffer. By the end of the incubation time, 10 μl fluorescent substrate (250 μM) were added to initiate the enzymatic reaction. The final reaction volume was 50 μl and the final concentration of drugs and substrate in the reaction mixture was 50 μM. After a second incubation period of 16–18 h, fluorescence was measured at 360/40 nm excitation and 460/40 nm emission using Synergy HT fluorescent plate reader. Drugs were screened from 0 to 1000 μM dose range to calculate the IC_{50}. To prepare positive control wells, 1% DMSO with 4 ng of enzyme and 50 μM of substrate were added without enzyme inhibitors. The standard lopinavir inhibitor was used at 50 μM

to serve as a positive control. Wells containing 1% DMSO with 50 μM of substrate without enzyme served as blanks. All the values were subtracted from blank values (see ESI† for manufacturer's kit (BPS Biosciences CA)).[64,65] The experiment was conducted at both room temperature (RT) and 37 °C.

Computational analysis methods

Molecular docking. To investigate the binding interaction of a target compound with the active site of SARS-CoV-2 M^{pro} enzyme, a molecular docking study was conducted using the Glide module of Schrodinger, associated with the graphical user interface program Maestro 8.[50,66] SARS-CoV2 M^{pro} protein crystal structure in complex with bipyridine benzonitrile was acquired from the RCSB Protein Data Bank (PDB) as entry code 7L11.[49] The protein preparation was completed in two steps: preparation and refinement, using Maestro 8.0's protein preparation wizard. After ensuring chemical correctness, water molecules in crystal structures were removed, and hydrogens were added wherever they were missing.[67–69] Using the OPLS 2005 forcefield, the energy of the crystal structure was minimized to avert any electronic clash in the structure. The binding site was specified around the co-crystallized ligand (Bipyridine benzonitrile), and the receptor grid was created using Grid Generation tool. Molecular docking was accomplished in standard precision mode using the glide ligand docking module. A single best pose is produced as the output for a specific ligand.[70]

Molecular dynamics (MD) simulation study. The thermodynamic stability of a promising molecule in complex with SARS-CoV-2 M^{pro} was evaluated using MD simulations on the OPLS3e forcefield with the Desmond package (Desmond 2020-3, Schrodinger LLC).[71] The ligand–protein complex was fixed in a solvent-soaked orthorhombic periodic box with a minimum distance of 10 Å between protein atoms and the box edges. The solvent was implemented using a single point charge (SPC) water model. The charge of the system was neutralized by adding Na^+ and Cl^- counter ions and 0.15 M NaCl Salt concentration was set corresponding to the physiological system using the Desmond 'System Builder' panel.[72,73] Then, the built solvated system was minimized and relaxed utilizing OPLS3e force field parameters as the default protocol associated with Desmond. The isothermal isobaric ensemble (normal pressure and temperature/NPT) was set during the simulation, with a temperature of 300 K and an atmospheric pressure of 1.0315 bar using the Nose–Hoover chain thermostat method and the Martyna–Tobias–Klein barostat method, respectively.[74,75] The MD simulation was carried out for a period of 100 ns, and trajectory snapshots were recorded at an interval of 20 ps. MD trajectories were investigated using Desmond's Simulation Interaction Diagram (SID) to predict the binding orientation of the ligand.

Author contributions

A. Aljuhani, H. E. A. Ahmed, and S. Ihmaid were responsible for the conception and rational design of the work. A. El-Agrody, A. M. Omar, M. F. Zayed, S. A. Salama, H. S. Abulkhair, and A. Aljuhani, were responsible for collection of data and synthesis of new compounds. S. Althagfan, Y. M. Alahmadi, S. Ahmed, and H. Ahmed, performed the molecular docking study. Molecular dynamic simulations have been conducted by H. E. A. Ahmed, S. Ihmaid, and A. A. Al-Karmalawy. A. El-Agrody, I. Ahma, M. A. Almikhlafi, S. H. Abulkhair, A. M. El-Agrody, S. A. Turkistani, M. Almaghrabi and, and H. S. Abulkhair were responsible for analyzing the spectral data and preparation of the ESI.† All authors read and approved the final form of the manuscript.

Conflicts of interest

The authors declare that there is no conflict of interest.

Acknowledgements

We greatly thank Taif University for providing fund for this work through Taif University Researcher Supporting Project number (TURSP-2020/52), Taif University, Taif, Saudi Arabia. We would also like to thank Professor Ali H. El-Far, Department of Biochemistry, Faculty of Veterinary Medicine, Damanhour University, Egypt, for his considerable help throughout revision stages of the manuscript.

References

1 P. Gautret, J.-C. Lagier, P. Parola, V. T. Hoang, L. Meddeb, M. Mailhe, B. Doudier, J. Courjon, V. Giordanengo, V. E. Vieira, H. Tissot Dupont, S. Honoré, P. Colson, E. Chabrière, B. La Scola, J.-M. Rolain, P. Brouqui and D. Raoult, *Int. J. Antimicrob. Agents*, 2020, **56**, 105949.
2 World Health Organization, *WHO Coronavirus (COVID-19) Dashboard*, **https://covid19.who.int/**, (accessed 7 July 2022).
3 A. R. Maher, M. Maglione, S. Bagley, M. Suttorp, J.-H. Hu, B. Ewing, Z. Wang, M. Timmer, D. Sultzer and P. G. Shekelle, *JAMA*, 2011, **306**, 1359.
4 A. Mahmoud, A. Mostafa, A. A. Al-Karmalawy, A. Zidan, H. S. Abulkhair, S. H. Mahmoud, M. Shehata, M. M. Elhefnawi and M. A. Ali, *Heliyon*, 2021, **7**, e07962.
5 M. I. A. Hamed, K. M. Darwish, R. Soltane, A. Chrouda, A. Mostafa, N. M. Abo Shama, S. S. Elhady, H. S. Abulkhair, A. E. Khodir, A. A. Elmaaty and A. A. Al-karmalawy, *RSC Adv.*, 2021, **11**, 35536–35558.
6 A. J. Pruijssers and M. R. Denison, *Curr. Opin. Virol.*, 2019, **35**, 57–62.
7 G. G. Plata, *The BMJ*, 2022, o1282.
8 A. Mahmoud, A. Mostafa, A. A. Al-Karmalawy, A. Zidan, H. S. Abulkhair, S. H. Mahmoud, M. Shehata, M. M. Elhefnawi and M. A. Ali, *Heliyon*, 2021, **7**, e07962.
9 O. Kutkat, Y. Moatasim, A. A. Al-Karmalawy, H. S. Abulkhair, M. R. Gomaa, A. N. El-Taweel, N. M. Abo Shama, M. GabAllah, D. B. Mahmoud, G. Kayali, M. A. Ali, A. Kandeil and A. Mostafa, *Sci. Rep.*, 2022, **12**, 12920.
10 L. Fu, F. Ye, Y. Feng, F. Yu, Q. Wang, Y. Wu, C. Zhao, H. Sun, B. Huang, P. Niu, H. Song, Y. Shi, X. Li, W. Tan, J. Qi and G. F. Gao, *Nat. Commun.*, 2020, **11**, 4417.

11 M. M. Hammoud, M. Khattab, M. Abdel-Motaal, J. Van der Eycken, R. Alnajjar, H. S. Abulkhair and A. A. Al-Karmalawy, *J. Biomol. Struct. Dyn.*, 2022, DOI: 10.1080/07391102.2022.2082533, https://www.tandfonline.com/doi/abs/10.1080/07391102.2022.2082533?journalCode=tbsd20.
12 A. A. Gaber, A. M. El-Morsy, F. F. Sherbiny, A. H. Bayoumi, K. M. El-Gamal, K. El-Adl, A. A. Al-Karmalawy, R. R. Ezz Eldin, M. A. Saleh and H. S. Abulkhair, *Arch. Pharm.*, 2021, DOI: 10.1002/ardp.202100258, https://onlinelibrary.wiley.com/doi/10.1002/ardp.202100258.
13 C. Choudhury, *J. Biomol. Struct. Dyn.*, 2021, **39**, 3733–3746.
14 I. Antonopoulou, E. Sapountzaki, U. Rova and P. Christakopoulos, *Comput. Struct. Biotechnol. J.*, 2022, **20**, 1306–1344.
15 Z. Jin, X. Du, Y. Xu, Y. Deng, M. Liu, Y. Zhao, B. Zhang, X. Li, L. Zhang, C. Peng, Y. Duan, J. Yu, L. Wang, K. Yang, F. Liu, R. Jiang, X. Yang, T. You, X. Liu, X. Yang, F. Bai, H. Liu, X. Liu, L. W. Guddat, W. Xu, G. Xiao, C. Qin, Z. Shi, H. Jiang, Z. Rao and H. Yang, *Nature*, 2020, **582**, 289–293.
16 K. Anand, J. Ziebuhr, P. Wadhwani, J. R. Mesters and R. Hilgenfeld, *Science*, 2003, **300**, 1763–1767.
17 S. Günther, P. Y. A. Reinke, Y. Fernández-García, J. Lieske, T. J. Lane, H. M. Ginn, F. H. M. Koua, C. Ehrt, W. Ewert, D. Oberthuer, O. Yefanov, S. Meier, K. Lorenzen, B. Krichel, J.-D. Kopicki, L. Gelisio, W. Brehm, I. Dunkel, B. Seychell, H. Gieseler, B. Norton-Baker, B. Escudero-Pérez, M. Domaracky, S. Saouane, A. Tolstikova, T. A. White, A. Hänle, M. Groessler, H. Fleckenstein, F. Trost, M. Galchenkova, Y. Gevorkov, C. Li, S. Awel, A. Peck, M. Barthelmess, F. Schlünzen, P. Lourdu Xavier, N. Werner, H. Andaleeb, N. Ullah, S. Falke, V. Srinivasan, B. A. França, M. Schwinzer, H. Brognaro, C. Rogers, D. Melo, J. J. Zaitseva-Doyle, J. Knoska, G. E. Peña-Murillo, A. R. Mashhour, V. Hennicke, P. Fischer, J. Hakanpää, J. Meyer, P. Gribbon, B. Ellinger, M. Kuzikov, M. Wolf, A. R. Beccari, G. Bourenkov, D. von Stetten, G. Pompidor, I. Bento, S. Panneerselvam, I. Karpics, T. R. Schneider, M. M. Garcia-Alai, S. Niebling, C. Günther, C. Schmidt, R. Schubert, H. Han, J. Boger, D. C. F. Monteiro, L. Zhang, X. Sun, J. Pletzer-Zelgert, J. Wollenhaupt, C. G. Feiler, M. S. Weiss, E.-C. Schulz, P. Mehrabi, K. Karničar, A. Usenik, J. Loboda, H. Tidow, A. Chari, R. Hilgenfeld, C. Uetrecht, R. Cox, A. Zaliani, T. Beck, M. Rarey, S. Günther, D. Turk, W. Hinrichs, H. N. Chapman, A. R. Pearson, C. Betzel and A. Meents, *Science*, 2021, **372**, 642–646.
18 I. Antonopoulou, E. Sapountzaki, U. Rova and P. Christakopoulos, *Comput. Struct. Biotechnol. J.*, 2022, **20**, 1306–1344.
19 D. S. Jairajpuri, A. Hussain, K. Nasreen, T. Mohammad, F. Anjum, M. Tabish Rehman, G. Mustafa Hasan, M. F. Alajmi and M. Imtaiyaz Hassan, *Saudi J. Biol. Sci.*, 2021, **28**, 2423–2431.
20 A. K. Ghosh, G. Gong, V. Grum-Tokars, D. C. Mulhearn, S. C. Baker, M. Coughlin, B. S. Prabhakar, K. Sleeman, M. E. Johnson and A. D. Mesecar, *Bioorg. Med. Chem. Lett.*, 2008, **18**, 5684–5688.
21 Z. Jin, Y. Zhao, Y. Sun, B. Zhang, H. Wang, Y. Wu, Y. Zhu, C. Zhu, T. Hu, X. Du, Y. Duan, J. Yu, X. Yang, X. Yang, K. Yang, X. Liu, L. W. Guddat, G. Xiao, L. Zhang, H. Yang and Z. Rao, *Nat. Struct. Mol. Biol.*, 2020, **27**, 529–532.
22 M. Negi, P. A. Chawla, A. Faruk and V. Chawla, *Bioorg. Chem.*, 2020, **104**, 104315.
23 A. K. Ghosh, G. Gong, V. Grum-Tokars, D. C. Mulhearn, S. C. Baker, M. Coughlin, B. S. Prabhakar, K. Sleeman, M. E. Johnson and A. D. Mesecar, *Bioorg. Med. Chem. Lett.*, 2008, **18**, 5684–5688.
24 D.-S. Park, E. Jo, J. Choi, M. Lee, S. Kim, H.-Y. Kim, J. Nam, S. Ahn, J. Y. Hwang and M. P. Windisch, *Eur. J. Med. Chem.*, 2017, **140**, 65–73.
25 M. Lee, J. Yang, E. Jo, J.-Y. Lee, H.-Y. Kim, R. Bartenschlager, E.-C. Shin, Y.-S. Bae and M. P. Windisch, *Sci. Rep.*, 2017, **7**, 44676.
26 K. Bafna, R. M. Krug and G. T. Montelione, *ChemRxiv*, 2020, DOI: 10.26434/chemrxiv.12153615.
27 K. Bafna, K. White, B. Harish, R. Rosales, T. A. Ramelot, T. B. Acton, E. Moreno, T. Kehrer, L. Miorin, C. A. Royer, A. García-Sastre, R. M. Krug and G. T. Montelione, *Cell Rep.*, 2021, **35**, 109133.
28 K. Bafna, K. White, B. Harish, R. Rosales, T. A. Ramelot, T. B. Acton, E. Moreno, T. Kehrer, L. Miorin, C. A. Royer, A. García-Sastre, R. M. Krug and G. T. Montelione, *Cell Rep.*, 2021, **35**, 109133.
29 R. Oerlemans, A. J. Ruiz-Moreno, Y. Cong, N. Dinesh Kumar, M. A. Velasco-Velazquez, C. G. Neochoritis, J. Smith, F. Reggiori, M. R. Groves and A. Dömling, *RSC Med. Chem.*, 2021, **12**, 370–379.
30 H. S. Abulkhair, A. Turky, A. Ghiaty, H. E. A. Ahmed and A. H. Bayoumi, *Bioorg. Chem.*, 2020, **100**, 103899.
31 M. H. El-Shershaby, K. M. El-Gamal, A. H. Bayoumi, K. El-Adl, H. E. A. Ahmed and H. S. Abulkhair, *Arch. Pharm.*, 2021, **354**, e2000277.
32 A. M. Omar, S. Ihmaid, E. S. E. Habib, S. S. Althagfan, S. Ahmed, H. S. Abulkhair and H. E. A. Ahmed, *Bioorg. Chem.*, 2020, **99**, 103781.
33 E. M. Othman, E. A. Fayed, E. M. Husseiny and H. S. Abulkhair, *New J. Chem.*, 2022, **46**, 12206–12216.
34 D. S. Jairajpuri, A. Hussain, K. Nasreen, T. Mohammad, F. Anjum, M. Tabish Rehman, G. Mustafa Hasan, M. F. Alajmi and M. Imtaiyaz Hassan, *Saudi J. Biol. Sci.*, 2021, **28**, 2423–2431.
35 M. Abass, M. Ismail, W. Abdel-Monem and A. Mayas, *Chem. Pap.*, 2010, **64**, DOI: 10.2478/s11696-009-0100-0, https://link.springer.com/article/10.2478/s11696-009-0100-0.
36 M. F. Maioral, C. do N. Bodack, N. M. Stefanes, Á. Bigolin, A. Mascarello, L. D. Chiaradia-Delatorre, R. A. Yunes, R. J. Nunes and M. C. Santos-Silva, *Biochimie*, 2017, **140**, 48–57.
37 M. H. El-Shershaby, A. Ghiaty, A. H. Bayoumi, A. A. Al-Karmalawy, E. M. Husseiny, M. S. El-Zoghbi and H. S. Abulkhair, *Bioorg. Med. Chem.*, 2021, **42**, 116266.
38 E. M. Othman, E. A. Fayed, E. M. Husseiny and H. S. Abulkhair, *Bioorg. Chem.*, 2022, **123**, 105762.

39 E. M. Othman, E. A. Fayed, E. M. Husseiny and H. S. Abulkhair, *Bioorg. Chem.*, 2022, **127**, 105968.
40 J. Osipiuk, S.-A. Azizi, S. Dvorkin, M. Endres, R. Jedrzejczak, K. A. Jones, S. Kang, R. S. Kathayat, Y. Kim, V. G. Lisnyak, S. L. Maki, V. Nicolaescu, C. A. Taylor, C. Tesar, Y.-A. Zhang, Z. Zhou, G. Randall, K. Michalska, S. A. Snyder, B. C. Dickinson and A. Joachimiak, *Nat. Commun.*, 2021, **12**, 743.
41 A. Abo Elmaaty, M. I. A. Hamed, M. I. Ismail, E. B. Elkaeed, H. S. Abulkhair, M. Khattab and A. A. Al-Karmalawy, *Molecules*, 2021, **26**, 3772.
42 T. Pillaiyar, M. Manickam, V. Namasivayam, Y. Hayashi and S.-H. Jung, *J. Med. Chem.*, 2016, **59**, 6595–6628.
43 R. L. Hoffman, R. S. Kania, M. A. Brothers, J. F. Davies, R. A. Ferre, K. S. Gajiwala, M. He, R. J. Hogan, K. Kozminski, L. Y. Li, J. W. Lockner, J. Lou, M. T. Marra, L. J. Mitchell, B. W. Murray, J. A. Nieman, S. Noell, S. P. Planken, T. Rowe, K. Ryan, G. J. Smith, J. E. Solowiej, C. M. Steppan and B. Taggart, *J. Med. Chem.*, 2020, **63**, 12725–12747.
44 C. Ma, Y. Hu, J. A. Townsend, P. I. Lagarias, M. T. Marty, A. Kolocouris and J. Wang, *ACS Pharmacol. Transl. Sci.*, 2020, **3**, 1265–1277.
45 W. Vuong, M. B. Khan, C. Fischer, E. Arutyunova, T. Lamer, J. Shields, H. A. Saffran, R. T. McKay, M. J. van Belkum, M. A. Joyce, H. S. Young, D. L. Tyrrell, J. C. Vederas and M. J. Lemieux, *Nat. Commun.*, 2020, **11**, 4282.
46 H. Abul-Khair, S. Elmeligie, A. Bayoumi, A. Ghiaty, A. El-Morsy and M. H. Hassan, *J. Heterocycl. Chem.*, 2013, **50**, 1202–1208.
47 A. K. Ghosh, M. Brindisi, D. Shahabi, M. E. Chapman and A. D. Mesecar, *ChemMedChem*, 2020, **15**, 907–932.
48 K. Sharun, R. Tiwari and K. Dhama, *Ann. Med. Surg.*, 2021, **61**, 122–125.
49 C.-H. Zhang, E. A. Stone, M. Deshmukh, J. A. Ippolito, M. M. Ghahremanpour, J. Tirado-Rives, K. A. Spasov, S. Zhang, Y. Takeo, S. N. Kudalkar, Z. Liang, F. Isaacs, B. Lindenbach, S. J. Miller, K. S. Anderson and W. L. Jorgensen, *ACS Cent. Sci.*, 2021, **7**, 467–475.
50 T. A. Halgren, R. B. Murphy, R. A. Friesner, H. S. Beard, L. L. Frye, W. T. Pollard and J. L. Banks, *J. Med. Chem.*, 2004, **47**, 1750–1759.
51 A. A. Zaki, M. M. Y. Kaddah, H. S. Abulkhair and A. Ashour, *RSC Adv.*, 2022, **12**, 2980–2991.
52 H. S. Abulkhair, S. Elmeligie, A. Ghiaty, A. El-Morsy, A. H. Bayoumi, H. E. A. Ahmed, K. El-Adl, M. F. Zayed, M. H. Hassan, E. N. Akl and M. S. El-Zoghbi, *Arch. Pharm.*, 2021, **354**, 2000449.
53 S. K. Ihmaid, A. Aljuhani, M. Alsehli, N. Rezki, A. Alawi, A. J. Aldhafiri, S. A. Salama, H. E. A. Ahmed and M. R. Aouad, *J. Mol. Struct.*, 2022, **1249**, 131568.
54 M. H. El-Shershaby, A. Ghiaty, A. H. Bayoumi, H. E. A. Ahmed, M. S. El-Zoghbi, K. El-Adl and H. S. Abulkhair, *New J. Chem.*, 2021, **45**, 11136–11152.
55 A. De, S. Sarkar and A. Majee, *Chem. Heterocycl. Compd.*, 2021, **57**, 410–416.
56 Y.-S. Chung, N.-J. Lee, S. H. Woo, J.-M. Kim, H. M. Kim, H. J. Jo, Y. E. Park and M.-G. Han, *Sci. Rep.*, 2021, **11**, 14817.
57 Genesig, *Coronavirus COVID-19 genesig® Real-Time PCR assay*, **https://www.genesig.com/assets/files/Path_COVID_19_CE_STED_IFU_Issue_500.pdf**, (accessed 12 March 2022).
58 T. Mosmann, *J. Immunol. Methods*, 1983, **65**, 55–63.
59 K. El-Adl, H. M. Sakr, R. G. Yousef, A. B. M. Mehany, H. S. Abulkhair and I. H. Eissa, *Arch. Pharm.*, 2022, **355**(7), 2200048, **https://onlinelibrary.wiley.com/doi/10.1002/ardp.202200048**.
60 K. El-Adl, M. K. Ibrahim, F. Khedr, H. S. Abulkhair and I. H. Eissa, *Arch. Pharm.*, 2022, **355**, 2100278.
61 F. Khedr, M. K. Ibrahim, I. H. Eissa, H. S. Abulkhair and K. El-Adl, *Arch. Pharm.*, 2021, **354**, e2100201.
62 K. El-Adl, H. Sakr, S. S. A. El-Hddad, A. G. A. El-Helby, M. Nasser and H. S. Abulkhair, *Arch. Pharm.*, 2021, **354**(7), DOI: **10.1002/ardp.202000491**, **https://onlinelibrary.wiley.com/doi/10.1002/ardp.202000491**.
63 W. Zhu, M. Xu, C. Z. Chen, H. Guo, M. Shen, X. Hu, P. Shinn, C. Klumpp-Thomas, S. G. Michael and W. Zheng, *Identification of SARS-CoV-2 3CL Protease Inhibitors by a Quantitative High-throughput Screening*, 2020.
64 L. Zhang, D. Lin, X. Sun, U. Curth, C. Drosten, L. Sauerhering, S. Becker, K. Rox and R. Hilgenfeld, *Science*, 2020, **368**, 409–412.
65 J. S. Morse, T. Lalonde, S. Xu and W. R. Liu, *ChemBioChem*, 2020, **21**, 730–738.
66 R. A. Friesner, R. B. Murphy, M. P. Repasky, L. L. Frye, J. R. Greenwood, T. A. Halgren, P. C. Sanschagrin and D. T. Mainz, *J. Med. Chem.*, 2006, **49**, 6177–6196.
67 K. El-Adl, A. G. A. El-Helby, H. Sakr, R. R. Ayyad, H. A. Mahdy, M. Nasser, H. S. Abulkhair and S. S. A. El-Hddad, *Arch. Pharm.*, 2021, **354**, e202000279.
68 H. G. Ezzat, A. H. Bayoumi, F. F. Sherbiny, A. M. El-Morsy, A. Ghiaty, M. Alswah and H. S. Abulkhair, *Mol. Diversity*, 2021, **25**, 291–306.
69 R. G. Yousef, H. M. Sakr, I. H. Eissa, A. B. M. Mehany, A. M. Metwaly, M. A. Elhendawy, M. M. Radwan, M. A. ElSohly, H. S. Abulkhair and K. El-Adl, *New J. Chem.*, 2021, **45**, 16949–16964.
70 I. Ahmad, M. Shaikh, S. Surana, A. Ghosh and H. Patel, *J. Biomol. Struct. Dyn.*, 2022, **40**, 3046–3059.
71 D. E. Shaw Research, 2021, **https://www.schrodinger.com/products/desmond**.
72 W. L. Jorgensen, D. S. Maxwell and J. Tirado-Rives, *J. Am. Chem. Soc.*, 1996, **118**, 11225–11236.
73 I. Ahmad, H. Jadhav, Y. Shinde, V. Jagtap, R. Girase and H. Patel, *In Silico Pharmacol.*, 2021, **9**, 23.
74 G. Kalibaeva, M. Ferrario and G. Ciccotti, *Mol. Phys.*, 2003, **101**, 765–778.
75 G. J. Martyna, *Phys. Rev. C: Nucl. Phys.*, 1994, **50**, 3234–3236.